Sensitivity Analysis

Oliwer Sliczniuk[a,*], Pekka Oinas[a]

[a]*Aalto University, School of Chemical Engineering, Espoo, 02150, Finland*

ARTICLE INFO

ABSTRACT

This study aimed to investigate the supercritical extraction process of caraway oil from chamomile flowers. The distributed-parameter model describes the fluid-solid extraction process. The concept of quasi-one-dimensional flow is applied to reduce the number of spatial dimensions. The flow is assumed to be uniform across any cross-section, although the area available for the fluid phase can vary along the extractor. The physical properties of the solvent are estimated from the Peng-Robinson equation of state. A set of laboratory experiments was performed under multiple constant operating conditions: $30 - 40°C$, $100 - 200$ bar, and $3.33 - 6.67 \times 10^{-5}$ kg/s. Sensitivity analyses play a crucial role in assessing the robustness of the findings or conclusions based on mathematical model. The local sensitivity analysis investigates the influence of infinitely small changes in the inlet temperature, pressure, and flow rate on the extraction yield.

1. Introduction

This study investigates the extraction of essential oil from chamomile flowers (Matricaria chamomilla L.) via supercritical fluid extraction techniques and the modelling of this process. Chamomile is a medicinal herb widely cultivated in southern and eastern Europe—such as Germany, Hungary, France, and Russia. It can be found outside of Europe in Brazil as discussed by Singh et al. [1]. This plant is distinguished by its hollow, bright gold cones, housing disc or tubular florets and surrounded by about fifteen white ray or ligulate florets. Chamomile has been used for its medicinal benefits, serving as an anti-inflammatory, antioxidant, mild astringent, and healing remedy. Chamomile's aqueous extract is widely used as a gentle sedative to calm nerves and mitigate anxiety, hysteria, nightmares, insomnia, and other sleep-related conditions, according to Srivastava [2]. Orav et al. [3] reported that oil yields from dried chamomile samples ranged from 0.7 to 6.7 mL/kg. Notably, the highest yields of essential oil, between 6.1 and 6.7 mL/kg, were derived from chamomile sourced from Latvia and Ukraine, while chamomile from Armenia exhibited a lower oil content of 0.7 mL/kg.

Evaluating the economic viability of the process is essential when choosing the suitable technology for essential oil extraction. Traditional methods, such as distillation and organic solvent extraction, are commonly employed but come with drawbacks. Distillation, for example, involves high temperatures that can lead to the thermal degradation of heat-sensitive compounds. This limitation has led to the increased popularity of alternative techniques like supercritical fluid extraction. Supercritical carbon dioxide is particularly appealing due to its distinctive properties: it is inflammable, non-toxic, and is non-corrosive. Moreover, compared to other fluids, its relatively low critical point positions it as an advantageous alternative to conventional extraction methods. Supercritical fluids are capable of exhibiting both gas- and liquid-like properties, allowing for adjustable dissolving power through changes in operating conditions.

The literature offers various mathematical models to detail the extraction of valuable compounds from a fixed biomass bed. Selecting a fitting model necessitates a deep understanding of the physical processes at play within the operational unit, as each model is built on specific assumptions and outlines distinct mass transfer mechanisms and equilibrium dynamics.

One model proposed by Reverchon et al. [4] is the hot ball model, which is based on an analogy to heat transfer and describes an extraction process from solid particles containing small quantities of solute where solubility is not a limiting factor.

The Broken-and-Intact Cell model, proposed by Sovova [5], assumes that external surfaces of particles are mechanically disrupted, allowing the solvent's access to the solute in broken cells, while the solute in intact cells remains less accessible due to higher mass transfer resistance.

Reverchon [6] formulated a fluid-solid extraction model where the solute is treated as a single component, governed by internal mass transfer resistance and omitting the effects of external mass transfer, axial dispersion, and variations in fluid density and flow rate throughout the bed.

This work builds upon the linear kinetic model suggested by Reverchon [6], deriving fundamental governing equations to develop a comprehensive model for the chamomile oil extraction process. This model aims for control-oriented simplicity, assuming a semi-continuous operation within a cylindrical vessel. The process involves supercritical solvent being pumped through a fixed bed of finely chopped biomass to extract the solute, followed by separation of the solvent and solute in a flush drum to collect the extract. Parameters such as the pressure (P), feed flow rate (F_{in}) and inlet temperature (T_{in}) are adjustable and measurable, while the outlet temperature (T_{out}) and the amount of product at the outlet can only be monitored. Figure

*Corresponding author

✉ oliwer.sliczniuk@aalto.fi (O. Sliczniuk)

ORCID(s): 0000-0003-2593-5956 (O. Sliczniuk); 0000-0002-0183-5558 (P. Oinas)

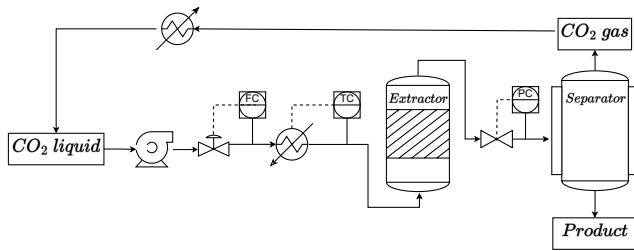[1](#) presents a simplified flow diagram illustrating the process setup.

Figure 1: Process flow diagram

This study focuses on creating a process model for the extraction of natural substances from solid materials using supercritical fluids, with a particular emphasis on supercritical CO_2. The approach involves estimating the solvent properties through thermodynamic relationships and determining the extraction kinetic parameters via a series of experiments conducted under a variety of conditions. The maximum likelihood estimator method is employed to address the parameter estimation challenge, with the derived parameters subsequently used to establish correlations. These correlations are instrumental in extending the applicability of the process model across different temperatures (30 to 40°C), pressures (100 to 200 bar) and flow rates (3.33 to 6.67 $\times 10^{-5}$ kg/s).

This study aims to analyze the influence of changes in operating conditions on the supercritical extraction process described in article 1. The emphasis is put on the effect of the mass flow rate, pressure, and the inlet temperature. The relation between input and output is obtained by applying a sensitivity analysis. Sensitivity analysis examines the impact of varying inputs or model parameters on the system's output. The aim is to understand and to allocate the source of uncertainty in the output to the corresponding inputs or parameters. There are many sensitivity analysis methods, which include but are not limited to those listed below:

- One-at-a-time method

- Derivative-based local methods

- Variance-based methods

Different supercritical extraction models were analyzed using sensitivity analysis. Fiori et al. [7], performed the sensitivity calculations by varying the parameters within their confidence interval and observing how the model results changed. This allows to evaluate the effect of the uncertainties on model predictions. The sensitivity analysis revealed that the particle diameter and the internal mass transfer coefficient are significant for the extraction process. The effect of changing some operative conditions was also investigated, underlining how the solvent flow rate and the seed milling affect the extraction process.

Santos et al. [8], in their work, considered a model of supercritical extraction process for semi-continuous isothermal and isobaric extraction process using carbon dioxide as a solvent. The parametric sensitivity analysis was carried out by applying disturbances of 10% in the values of the normal operation conditions.

Hatami and Ciftci [9] used a one-factor-at-a-time sensitivity analysis to assess the response of NPV concerning variations in both technical and economic variables. Their findings show that the most influential factors on NPV include the price of the extract, the interest rate, the dynamic time of SFE, and the project lifetime.

Poletto and Reverchon [10] provided a general dimensionless model for the supercritical extraction process of vegetable and essential oils and applied a sensitivity analysis. They found that a dimensionless partition coefficient and a dimensionless characteristic time appeared as the most important parameters of the extraction process. The sensitivity calculations were performed by varying the parameters and analyzing the model response.

2. Materials and methods

2.1. Supercritical fluids

A supercritical fluid (SCF) is a substance at a temperature and pressure above its critical point, where there are no distinct liquid and gas phases but below the pressure required to compress it into a solid. SCFs can move through porous solids like gases, which is faster than liquid transport through such materials. SCFs have a higher ability to dissolve materials like liquids or solids compared to gases. Near the critical point, small changes in pressure or temperature result in significant changes in density, allowing many properties of an SCF to be fine-tuned. By changing the pressure and temperature, the properties of carbon dioxide can be tuned to be more liquid-like or gas-like.

Fluid properties can be divided into two kinds: equilibrium properties and transport properties. The equation of state can be used accurately to predict the equilibrium properties, such as fluid density, enthalpy, vapour pressure, fugacity and fugacity coefficient, vapour-liquid equilibrium, and all kinds of excess properties.

Supercritical CO_2's thermodynamic properties, such as density or specific heat capacity, vary significantly with slight changes in temperature and pressure due to real gas effects. The Peng-Robinson equation of state (P-R EOS) is used to calculate the thermodynamic properties by accounting for these real gas effects are presented in Appendix **??**. The P-R EOS belongs to a specific class of thermodynamic models for modelling the pressure of a solvent as a function of temperature and density and which can be rewritten as a cubic function of the molar volume.

To determine the thermodynamic properties of a real gas, it is necessary to evaluate the departure function of the chosen equation of state for that property. As explained by Elliott [11], the departure function describe the difference between the actual value of a thermodynamic property of a real gas and its value if the gas were ideal under the same temperature and pressure conditions. The ideal gas serves as a reference state to which the properties of real gases

are compared. The departure function measures the extent to which a real gas deviates from ideal gas behaviour. The departure functions allow for the accurate calculation of thermodynamic properties for real gases.

The properties of CO_2 are presented as a function of operating conditions (temperature and pressure) in Figure 2. At standard atmospheric pressure and temperature, CO_2 behaves as an ideal gas, and its compressibility factor equals unity. However, at high pressures and/or low temperatures, intermolecular forces between gas molecules become more significant, causing them to deviate from ideal behaviour. As a result, the compressibility factor can be greater than or less than unity, depending on the magnitude of these forces. As presented in Figure 2a, the compressibility factor obtained from the Peng-Robinson equation of state varies strongly depending on the operating conditions.

The real gas effects are also visible on the density plot presented in Figure 2b. The density calculations are based on the compressibility factor, and its value depends on the operating conditions. The fluid properties near the critical point are unique and combine gas-like and liquid-like properties. The details of calculations are explained in Appendix **??**.

Figure 2c show the behaviour of the heat capacity of a supercritical fluid at constant pressure (C_p). The details of the calculations can be found in Appendix **??**. Contrary to the density, which varies monotonically, the specific heat shows very high levels in a narrow region. In the subcritical region, the phase transition is associated with an effective spike in the heat capacity (i.e., the latent heat). Approaching the critical point, the latent heat falls to zero, which is accompanied by a gradual rise in heat capacity in the pure phases near phase transition. At the critical point, the latent heat is zero, but the heat capacity shows a diverging singularity. Beyond the critical point, there is no divergence, but rather a peak in the heat capacity; the highest point of this peak identifies the Widom line (as discussed by Simeoni et al. [12] and Banuti [13]).

Figure 2d represent how the specific enthalpy change with the operating conditions. The details of calculations are discussed in Appendix **??**.

Transport properties such as viscosity and conductivity play a crucial role in engineering design for production, fluid transportation, and processing. However, as highlighted by Sheng et al. [14], developing a satisfactory theory for transport properties of real dense gases and liquids is a challenging task. This is due to the inherent difficulties involved in accurate measurements and the complexity involved in theoretical treatments.

To address this issue, the correlations of transport coefficients are either empirical or based on some theoretical foundation. Chapman-Enskog's theory (presented in Chapman and Cowling [15]) for transport properties of dense gases based on the distribution function is a popular theoretical approach. However, the Chapman-Enskog theory was developed for rigid spherical molecules and modifications are required to apply it to real gases. Many correlations have

been proposed following the Chapman-Enskog theory in the form of reduced density and reduced temperature, such as those developed by Fenghour et al. [16], and Laesecke and Muzny [17] from the National Institute of Standards and Technology (NIST). The correlation of Laesecke and Muzny [17] is presented in Figure 2e.

NIST has developed a viscosity formulation consisting of four contributions: (i) for the limit of zero density, (ii) for the initial density dependence, (iii) for the residual viscosity, and (iv) for the singularity of the viscosity at the critical point. The NIST correlation covers temperatures from 100 to 2000 K for gaseous CO_2, and from 220 to 700 K with pressures along the melting line up to 8000 MPa for compressed and supercritical liquid states. These correlations and theories are essential in predicting transport properties for real gases and liquids and can assist in engineering design and analysis.

Similarly, the NIST developed the correlation, which describe the behaviour of thermal diffusivity of CO_2. The work of Huber et al. [18] captures the singular behaviour of thermal conductivity around the critical point. The correlation is applicable for the temperature range from the triple point to 1100 K and pressures up to 200 MPa. Figure 2f shows how the thermal conductivity of carbon dioxide change depending on the operating conditions.

2.2. Governing equations

The governing equation for a quasi-one-dimensional compressible flow in Cartesian coordinates can be found in the Appendix **??** and in the work of Anderson [19]. Quasi-one-dimensional flow is a fluid flow characterized by the assumption that the flow properties remain uniform across any given cross-section of the flow. This assumption is made when there is a variation in the cross-sectional area of the flow channel, such as an irregular shape or partial filling of an extractor. In such cases, the flow is considered to be quasi-one-dimensional because the velocity and other flow properties are assumed to vary only in the direction of flow.

The quasi-one-dimensional compressible Navier-Stokes equations in Cartesian coordinates are given by Equations 1 to 3. The derivation of these Equations are presented in Appendix **??**.

$$\frac{\partial \left(\rho_f A_f(z) \right)}{\partial t} + \frac{\partial \left(\rho_f A_f(z) v \right)}{\partial z} = 0 \tag{1}$$

$$\frac{\partial \left(\rho_f v A_f(z) \right)}{\partial t} + \frac{\partial \left(\rho_f A_f(z) v^2 \right)}{\partial z} = -A_f(z) \frac{\partial P}{\partial z} \tag{2}$$

$$\frac{\partial \left(\rho_f e A_f(z) \right)}{\partial t} + \frac{\partial \left(\rho_f A_f(z) v e \right)}{\partial z} = -P \frac{\left(A_f(z) v \right)}{\partial z} + \frac{\partial}{\partial z} \left(\frac{\partial T}{\partial z} \right) \tag{3}$$

where ρ_f is the density of the fluid, $A_f(z)$ is the function which describe change of the cross-section, v is the velocity, P is the total pressure, e is the internal energy of the fluid, t is time and z is the spacial direction.

Based on governing equations, the small discontinuity (defined as δ) in flow properties, shown in Figure 3, can be analysed. The analysis follows the work of Schreier [20].
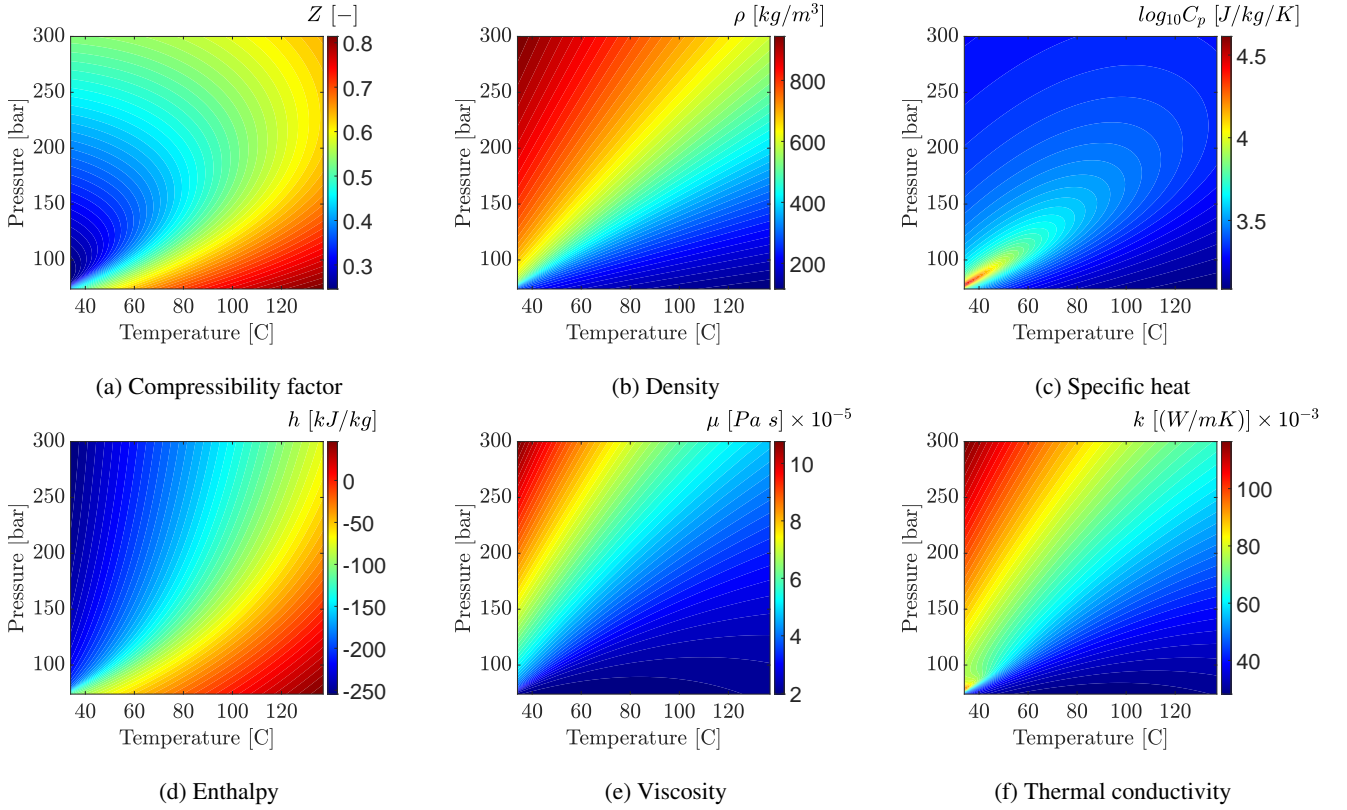
Figure 2: Properties of CO_2 based on the equation of state and correlations

	ρ_f	$\rho_f + \delta\rho_f$	
$v \rightarrow$	P	$P + \delta P$	$v + \delta v \rightarrow$
	T	$T + \delta T$	

Figure 3: Small discontinuity in one-dimensional flow

The discontinuity is presumed to be at rest relative, and the balance equations become

$$\rho_f \delta v + v \delta \rho_f + \delta \rho_f \delta v = 0$$

$$\delta P = \delta v \delta \rho_f$$

These relations are equally valid if the two regions are separated by a region of finite width rather than a discontinuity.

$$\lim_{\rho_f v \to 0} \rho_f \delta v + v \delta \rho_f + \delta \rho_f \delta v = 0/\delta \rho_f \rightarrow \frac{dv}{d\rho_f} = -\frac{v}{\rho_f}$$

By combining the momentum equation with the above equation, we get

$$\frac{dv}{d\rho_f} = -\frac{dv}{dP}\frac{dP}{d\rho_f} = -\frac{1}{\rho v}\frac{dP}{d\rho_f} = -\frac{v}{\rho_f} \tag{4}$$

Suppose the flow is presumed to be isentropic, $dP/d\rho_f = c^2$, so $v^2 = c^2$, where c is the speed of sound. This can be interpreted as a small pressure wave propagating with the speed of sound relative to the flow. Moreover, if the flow velocity is relatively low, all pressure changes are hydrodynamic (due to velocity motion) rather than thermodynamic

which leads to $\partial \rho_f / \partial P \approx 0$. In other words, the small changes in pressure due to flow velocity changes do not change the density.

2.3. Extraction model
2.3.1. Continuity equation

The obtained above quasi-one-dimensional continuity equation (Equation 1) is further modified by specifying a function $A_f(z) = A\phi(z)$ to take into account the change of the cross-section available for the fluid. The Equation 5 shows the differential form of the continuity equation:

$$\frac{\partial(\rho_f(T(t,z), P(t))\phi(z))}{\partial t} + \frac{\partial(\rho_f(T(t,z), P(t))vA\phi(z))}{\partial z} = 0 \tag{5}$$

where A is the total cross-section of the extractor and $\phi(z)$ describe porosity along the extractor.

Assuming that the mass flow rate is constant in time, the temporal derivative becomes zero, and the spatial derivative can be integrated along z as

$$\int \frac{\partial(\rho_f(T(t,z), P(t))vA\phi(z))}{\partial z} dz = 0 \rightarrow F = \rho_f(T(t,z), P(t))vA\phi(z) \tag{6}$$

Here, F is a constant obtained from the integration and is understood as the mass flux per unit area, which is assumed to be constant along z. To simplify the dynamics of the system, it is assumed that $F = F(t)$ is a control variable and affects the whole system instantaneously. This assumption allows for finding the velocity profile that satisfies mass continuity based on $F(t)$, $\phi(z)$, and $\rho_f(T(t,z), P(t))$.

$$v = \frac{F(t)}{\rho_f(T(t,z), P(t)) A \phi(z)} \quad (7)$$

The fluid density $\rho_f(T(t,z), P(t))$ can be obtained from an equation of state if temperature and the thermodynamic pressure (assumed $P(t)$ to be constant along z due to the low-Mach number condition) are known. The variation in density may be caused by the fluid accumulation in the system (equivalent to pressure change), which occurs instantaneously along z or by a temperature change.

Analogously, the superficial velocity might be introduced to the model and defined as

$$u = v\phi(z) = \frac{F(t)}{\rho_f(T(t,z), P(t)) A} \quad (8)$$

2.3.2. Mass balance for the fluid phase

The detailed derivation of the mass balance equation for the fluid phase can be found in Appendix **??**. The movement of the pseudo-homogeneous fluid phase (Equation 9) is considered only in the axial direction due to quasi-one-dimensional assumptions, which take into account variation of the void fraction. Furthermore, the thermodynamic pressure is assumed to be constant along the device as presented by Equation 4. Additionally, the boundary layer adjacent to the inner wall of the extractor is neglected, resulting in a constant velocity profile across any cross-section of the extractor perpendicular to the axial direction. The amount of solute in the solvent is considered negligible, resulting in the fluid phase being described as pseudo-homogeneous, and its properties are assumed to be the same as the solvent. The mass balance equation for the fluid phase includes convection, diffusion, and kinetic terms.

$$\frac{\partial c_f(t,z)}{\partial t} + \frac{1}{\phi(z)} \frac{\partial \left(c_f(t,z) u \right)}{\partial z} = \frac{1 - \phi(z)}{\phi(z)} r_e(t,z) + \frac{1}{\phi(z)} \frac{\partial}{\partial z} \left(D_e^M \frac{\partial c_f(t,z)}{\partial z} \right) \quad (9)$$

$c_f(t,z)$ represents the concentration of solute in the fluid phase, , $r_e(t,z)$ is a mass transfer kinetic term, and $D_e^M(T(t,z), P(t), F(t))$ is the axial mass diffusion coefficient.

2.3.3. Mass balance for the solid phase

The solid phase is considered to be stationary, with negligible convection and diffusion terms in the mass balance equation (Equation 10). Therefore, the only significant term in this equation is the kinetic term (as defined in Equation 11), which connects the solid and fluid phases. The extract is represented by a single pseudo-component to simplify the analysis.

$$\frac{\partial c_s(t,z)}{\partial t} = \underbrace{r_e(t,z)}_{\text{Kinetics}} \quad (10)$$

2.3.4. Kinetic term

The kinetic term in this study is based on the two-film theory proposed by Reverchon [6], and the mass transfer kinetic is given by Equation 11. This equation takes into account the overall diffusion coefficient and the concentration gradient, which acts as the driving force for the process.

As the solvent flows through the bed, CO_2 molecules diffuse into the pores and adsorb on the particle surface to form an external fluid film around the solid particles due to the solvent-solid matrix interactions. The effect of Knudsen diffusion is negligible in this process, as the mean free path of the molecule is much smaller than the pore diameter. The dissolved solute diffuses from the particle's core through the solid-fluid interface, the pore, and the film into the bulk. Figure 4 illustrates the mass transfer mechanism, where the mean solute concentration in the solid phase is denoted as c_s and the equilibrium concentrations at the solid-fluid interface are denoted as c_s^* and c_p^*, respectively, for solid and fluid phases. The concentration of the solutes in the fluid phase in the center of the pore is denoted as c_p. As the solute diffuses through the pore, its concentration changes and reaches c_{pf} at the opening of the pore. The solute then diffuses through the film around the particle and reaches a concentration in bulk c_f. The two-film theory describes the solid-fluid interface inside the pore. The overall mass transfer coefficient can be determined if the relationship between the solute concentration in one phase and its equilibrium concentration is known.
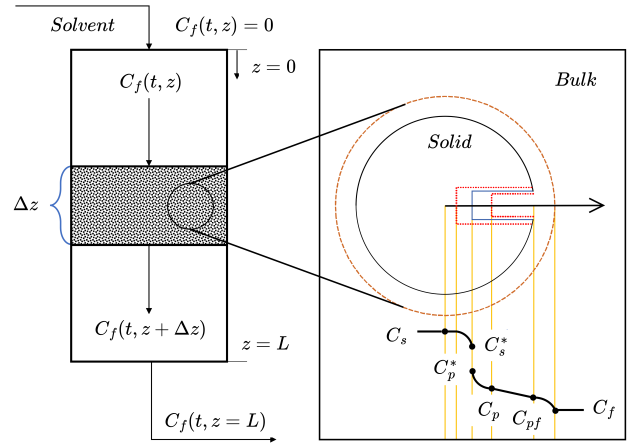

Figure 4: The extraction mechanism

Bulley et al. [21] suggests a process where the driving force for extraction is given by the difference between the concentration of the solute in bulk, c_f, and in the center of the pore, c_p^*. The concentration c_p^* is in equilibrium with c_s according to an equilibrium relationship. The rate of extraction is thus $r_e \left(c_f - c_p^*(c_s) \right)$.

On the other hand, Reverchon [6] proposes a driving force given by the difference between c_s and c_p^*. c_p^* is determined by an equilibrium relationship with c_f and the extraction rate is $r_e \left(c_s - c_p^*(c_f) \right)$ or more precisely

$$r_e(t,z) = \frac{D_i(T(t,z), P(t))}{\mu l^2} \left(c_s(t,z) - c_P^*(t,z) \right) \quad (11)$$

where μ is sphericity, l a characteristic dimension of particles and can be defined as $l = r/3$, r is the mean particle

radius, ρ_s is the solid density, $D_i(T(t, z))$ corresponds to the overall diffusion coefficient and $c_P^*(t, z)$ is a concentration at the solid-fluid interface (which according to the internal resistance model is supposed to be at equilibrium with the fluid phase).

According to Bulley et al. [21], a linear equilibrium relationship (equation 12) can be used to find an equilibrium concentration of the solute in the fluid phase $c_f^*(t, z)$ is based on the concentration of the solute in the solid phase $c_s(t, z)$

$$c(t, z) = k_p(T(t, z), P(t))q^*(t, z) \qquad (12)$$

The volumetric partition coefficient $k_p(T(t, z), P(t))$ behaves as an equilibrium constant between the solute concentration in one phase and the corresponding equilibrium concentration at the solid-fluid interphase. According to Spiro and Kandiah [22], the term $k_p(T(t, z), P(t))$ can be expressed as the function of mass partition factor $k_m(T(t, z))$.

$$k_m(T(t, z)) = \frac{k_p(T(t, z), P(t))\rho_s}{\rho(T(t, z), P(t))} \qquad (13)$$

Equation 14 represents of the kinetic term according to Reverchon [6]

$$r_e(t, z) = -\frac{D_i(T(t, z), P(t))}{\mu l^2}\left(c_s(t, z) - \frac{\rho_s}{k_m(T(t, z))\rho_f(T(t, z), P(t))}c_f(t, z)\right) \qquad (14)$$

2.3.5. Uneven distribution of the solute in the solid phase

Following the idea of the Broken-and-Intact Cell (BIC) model presented by Sovova [23], the internal diffusion coefficient D_i is consider to be a product of the reference value of D_i^R and the exponential decay function γ, as given by Equation 15.

$$D_i = D_i^R \gamma(c_s(t, z)) = D_i^R \exp\left(\Upsilon\left(1 - \frac{c_s(t, z)}{c_{s0}}\right)\right) \qquad (15)$$

where the Υ describe the curvature of the decay function. The final form of the extraction kinetic Equation is given by Equation 16.

$$r_e(t, z) = -\frac{D_i^R(T(t, z), P(t))\gamma(c_s(t, z))}{\mu l^2}\left(c_s(t, z) - \frac{\rho_s}{k_m(T(t, z))\rho(T(t, z), P(t))}c_f(t, z)\right) \qquad (16)$$

Such a formulation limits the availability of the solute in the solid phase. Similarly to the BIC model, if solute is assumed to be contained in the cells, a part of which is open because the cell walls were broken by grinding, and the rest remains intact. The diffusion of the solute from a particle's core takes more time compared to the diffusion of the solute located close to the outer surface. Considering that the internal diffusion coefficient decay as the concentration of the solute in the solid decrease. As the value of the c_s decrease over time, the exponential term approach unity and $\lim_{c_s \to 0} D_i = D_i^R$. D_i^R can be interpreted as the internal diffusion coefficient at vanishing gradient.

Alternatively, the decay function γ can be consider with respect to the Shrinking Core model presented by Goto et al.

[24], where the particle radius change as the amount of solute in the solid phase decrease. As the particle size decrease due to dissolution, the diffusion path increase which makes the diffusion slower and reduce the value of a diffusion coefficient. The same analogy can be apply to the Equation 15 to explain the change of the diffusion coefficient.

2.3.6. Heat balance

The heat governing equation describe the evolution of the energy in the system and it is given by 17. The derivation of the heat equation can be found in Appendix ??.

$$\frac{\partial\left(\rho_f(T(t, z), P(t))e(t, z)A_f\right)}{\partial t} + \frac{\partial\left(\rho_f(T(t, z), P(t))A_f ve(t, z)\right)}{\partial z}$$
$$= -P(t)\frac{(A_f v)}{\partial z} + \frac{\partial}{\partial z}\left(\frac{\partial T(t, z)}{\partial z}\right) \qquad (17)$$

The departure function is a mathematical function that characterizes the deviation of a thermodynamic property (enthalpy, entropy, and internal energy) of a real substance from that of an ideal gas at the same temperature and pressure. The departure function is typically defined as the difference between the value of a thermodynamic property for a real fluid and the corresponding value for an ideal gas at the same temperature and pressure. They are typically computed by integrating a function that depends on the equation of state and its derivatives. Following Elliott [11] or Gmehling et al. [25], a real gas internal energy definition can be obtained from the departure functions, defined through Equation 18. More information on the departure functions can be found in Appendix ??.

$$de(t, z) = C_v dT - \left[P(t) - T(t, z)\left(\frac{\partial P(t)}{\partial T(t, z)}\right)_{v_m(T(t, z), P(t))}\right]dv_m(T(t, z), P(t)) \qquad (18)$$

where $e^{id}(t, z)$ is the internal energy of perfect gas.

Suppose a gas is considered to be perfectly caloric $(e(t, z) = C_v T(t, z))$, then the energy equation can be written explicitly in the form of temperature. The perfectly caloric gas can be seen as the special case of a real gas, where the second term of Equation 18 goes to zero and the heat capacity C_v is constant.

For real gases, it is complicated to write the heat balance in terms of temperature, but it be can be used directly in the form of internal energy, as it is given by Equation 3. In such a case, the temperature needs to be recovered from the internal energy. A relation for the internal energy can be obtained from an equation of state. For Peng-Robinson, such a relation is given by Equation 19 as presented by Elliott [11].

$$\frac{e(t, z) - e^{id}(t, z)}{RT(t, z)} =$$
$$-\frac{A(T(t, z), P(t))}{B(T(t, z), P(t))\sqrt{8}}\frac{\kappa\sqrt{T_r}}{\sqrt{\alpha}}\ln\left[\frac{Z(T(t, z), P(t)) + \left(1 + \sqrt{2}\right)B(T(t, z), P(t))}{Z(T(t, z), P(t)) + \left(1 - \sqrt{2}\right)B(T(t, z), P(t))}\right] \qquad (19)$$

To solve Equation 19, temperature, pressure, and density values need to be known. If an equation of state is

introduced, then only two out of three variables need to be obtained as the third one can be calculated; this can be represented as follow

$$e(t,z) = e(T(t,z), P(t), \rho_f(T(t,z), P(t))) = e(T(t,z), P(t), \rho_f(T(t,z), P(t))) \tag{20}$$

If the value of internal energy $e(t,z)$ is known from the time evolution of the energy Equation 3, and pressure is known from measurement, then the temperature can be reconstructed. A roootfinder can be used to find a value of temperature, which minimizes the difference between the value of internal energy coming from the time evolution (Equation 17) and the output from Equation 19. Such a procedure allow to find local temperature along spatial direction z and needs to be repeated every time-step.

Another way to express the energy equation is to introduce enthalpy $h(t,z) = e(t,z) + P(t)/\rho_f(T(t,z), P(t))$. By introducing the definition of enthalpy, the energy equation becomes

$$\frac{\partial \left(\rho_f(T(t,z), P(t))h(t,z)A_f \right)}{\partial t} - \frac{\partial \left(P(t)A_f \right)}{\partial t}$$
$$+ \frac{\partial \left(\rho_f(T(t,z), P(t))h(t,z)A_f v \right)}{\partial z} - \frac{\partial}{\partial z}\left(k\frac{\partial T(t,z)}{\partial z} \right) \tag{21}$$

The main advantage of this formulation is the presence of term $\partial P(t)/\partial t$, which allows it to directly affect the system through the change of thermodynamic pressure (which is a control variable). The enthalpy is related to the pressure and temperature through the following equation:

$$h(t,z) = h(T(t,z), P(t), \rho_f(T(t,z), P(t))) = h(T(t,z), P(t), \rho_f(T(t,z), P(t))) \tag{22}$$

If the value of enthalpy is known from the time evolution and pressure can be measured, then the Equation 22 can be solved for the temperature to recover the temperature profile. For the Peng-Robinson EoS, the enthalpy can be defined by Equation 23. More details can be found in Appendix **??** or given by Gmehling et al. [25].

$$h(t,z) - h(t,z)^{id} = RT(t,z)\left[T_r(Z(T(t,z), P(t)) - 1) \right.$$
$$\left. -2.078(1+\kappa)\sqrt{\alpha(T(t,z))} \ln\left(\frac{Z(T(t,z), P(t)) + \left(1+\sqrt{2}\right) B(T(t,z), P(t))}{Z(T(t,z), P(t)) + \left(1-\sqrt{2}\right) B(T(t,z), P(t))} \right) \right] \tag{23}$$

The Equation 23 requires an reference sate, which in this case is assumed to be $T_{ref} = 298.15$ [K] and $P_{ref} = 1.01325$ [bar].

As discussed by Gmehling et al. [25], the influence of the intermolecular forces on the enthalpy is needs to taken into account in high pressures systems. In most cases, these forces are attractive, so additional energy is necessary to move the molecules away from each other, that is, to lower the density. If this energy is not added, the substance cools down when it is expanded.

2.3.7. Pressure term

The pressure term in the energy equation, given by Equation 21, describes the change of the thermodynamic pressure with respect to time. As explained in Chapters 2.2, at Low-Mach number conditions, the thermodynamic pressure is nearly constant in space due to the small pressure wave propagation that occurs at the speed of sound. Under such conditions, the term $\partial P/\partial t$ can be approximated by an ordinary differential equation, which describes the instantaneous change of pressure in the system. The pressure (P) in the system is considered a state variable, while the pressure in the new time-step (P_{in}) is considered a control variable.

$$\frac{\partial P(t)}{\partial t} \approx \frac{P(t) - P_{in}(t)}{\Delta t} \tag{24}$$

Such a simplified equation takes into account the pressure change in the energy balance, but the dynamics are simplified and do not consider the effects of pressure losses. In a real system, the dynamics of pressure change would depend on a pump used in an extraction system, as well as a back-pressure regulator used to control an outlet valve.

2.3.8. Extraction yield

The efficiency of the process (the yield) is calculated according to Equation 25 as presented by Sovova et al. [26]. The measurement equation evaluate the mass of solute at the outlet of the extraction unit and sums it. The integral form of the measurement equation (25) can be transformed into the differential form (26) and augmented with the process model.

$$y(t) = \int_{t_0}^{t_f} \frac{F(t)}{\rho_f(T(t,z), P(t))} c_f(t,z) \bigg|_{z=L} dt \tag{25}$$

$$\frac{dy(t)}{dt} = \frac{F(t)}{\rho_f(T(t,z), P(t))} c_f(t,z) \bigg|_{z=L} \tag{26}$$

2.3.9. Initial and boundary conditions

It is assumed that the solvent is free of solute at the entrance of the extractor and that all the solid particles have the same initial solute content c_{s0}. Every SFE system needs some time to reach the desired operating conditions but the solute diffuses from solid phase to the fluid phase already at the preparation stage. For instance, a pump introduce more fluid to the extractor to increase the pressure, which makes the fluid present already in that vessel to moves internally hence the solute in the fluid phase is non-uniformly distributed. Some conclusions can be drawn from the analysis of the initial part of each yield curve obtained from the laboratory (Figure **??**). It can be noticed that each curve at the beginning has a non-linear curvature. A quadratic function could approximate the initial part of each extraction curve. A function that, after integration, gives a quadratic-like result is a straight line. Based on that observation, the solute concentration in the fluid phase is assumed to be linearly distributed. The solute concentration is assumed to be zero at the outlet and reach the maximum at the beginning of the fixed bed. The details on the calculation are given in Appendix **??**. The linear distribution $H(z)$ can be defined if the total mass of solute m_{total} and initial mass ratio between solid and fluid phases τ are known. Moreover, it is considered that the initial temperature of the extractor in every place is the same and described by h_0. Therefore, the initial conditions employed in the simulation are:

$$c_f(t=0,z) = H(z) \quad c_s(t=0,z) = c_{s0} \quad h(t=0,z) = h_0$$

2.3.10. State-space representation

The process model can be written in a general form:

$$
\begin{bmatrix}
\dfrac{\partial c_f(t,z)}{\partial t} \\[6pt]
\dfrac{\partial c_s(t,z)}{\partial t} \\[6pt]
\dfrac{\partial h(t,z)}{\partial t} \\[6pt]
\dfrac{\partial P(t,z)}{\partial t} \\[6pt]
\dfrac{\partial y(t)}{\partial t}
\end{bmatrix}
=
\begin{bmatrix}
\bar{\phi}_1\left(c_f(t,z),c_s(t,z),h(t,z);\Theta\right) \\
\bar{\phi}_2\left(c_f(t,z),c_s(t,z),h(t,z);\Theta\right) \\
\bar{\phi}_3\left(c_f(t,z),c_s(t,z),h(t,z);\Theta\right) \\
\bar{\phi}_4\left(c_f(t,z),c_s(t,z),h(t,z);\Theta\right) \\
\bar{\phi}_5\left(c_f(t,z),c_s(t,z),h(t,z);\Theta\right)
\end{bmatrix}
= \bar{\phi}(t,z;\Theta) = \dfrac{\partial \chi(t,z)}{\partial t}
$$

$$(27)$$

where Θ is a paramter space, $\bar{\phi}$ is a set of functions that correspond to state equations of the model, and χ is the state-space model.

Function $\bar{\phi}$ are transformed to a corresponding set of N_z discretized equations denoted as G. The state-space model $\chi(t,z)$ after the discretization is represented by $\dot{x}(t)$.

$$
\dot{x}(t) = \frac{dx(t)}{dt} =
\begin{bmatrix}
\dfrac{dc_{f,1}(t)}{dt} \\[4pt]
\vdots \\[4pt]
\dfrac{dc_{f,N_z}(t)}{dt} \\[8pt]
\dfrac{dc_{s,1}(t)}{dt} \\[4pt]
\vdots \\[4pt]
\dfrac{dc_{s,N_z}(t)}{dt} \\[8pt]
\dfrac{dh_1(t)}{dt} \\[4pt]
\vdots \\[4pt]
\dfrac{dh_{N_z}(t)}{dt} \\[8pt]
\dfrac{dP(t)}{dt} \\[8pt]
\dfrac{dy(t)}{dt}
\end{bmatrix}
=
\underbrace{
\begin{bmatrix}
G_1\left(c_f(t),c_s(t),h(t);\Theta\right) \\
\vdots \\
G_{N_z}\left(c_f(t),c_s(t),h(t);\Theta\right) \\[6pt]
G_{N_z+1}\left(c_f(t),c_s(t),h(t);\Theta\right) \\
\vdots \\
G_{2N_z}\left(c(t),c_s(t),h(t);\Theta\right) \\[6pt]
G_{2N_z+1}\left(c_f(t),c_s(t),h(t);\Theta\right) \\
\vdots \\
G_{3N_z}\left(c_f(t),c_s(t),h(t);\Theta\right) \\[6pt]
G_{3N_z+1}\left(c_f(t),c_s(t),h(t);\Theta\right) \\[6pt]
G_{3N_z+2}\left(c_f(t),c_s(t),h(t);\Theta\right)
\end{bmatrix}
}_{G(x(t);\Theta)}
$$

where $x \in \mathbb{R}^{N_x=3N_z}$ and $\Theta \in \mathbb{R}^{N_\Theta=N_\theta+N_u}$, N_θ is the number of model parameters, N_u is the number of control variables.

In a state-space sense, the state variables of the system are the local concentrations of solute in the fluid and solid phases ($c_f(t,z)$ and $c_s(t,z)$, respectively), and the local enthalpy of the pseudo-homogeneous phase ($h(t,z)$). The controllable input variables are the mass flow-rate and temperature of the solvent in the feed and the pressure in the extractor. Additionally, the pressure change is augmented with the state-space and denoted as $P(t)$. The system state-space is extended by assuming that extraction yield can be modelled as a function of a known initial mass of solute in the solid phase and it can be measured after the separator

($Y(t)$). The system is controllable by manipulating the flow-rate and temperature (enthalpy) of CO_2 in the feed, and the pressure in the extractor.

2.3.11. Discretization methods

The method of lines is used to transform the process model equations into a set of ODEs denoted as $G(x(t);\Theta)$. The partial derivatives in z-direction are computed using a first-order and second-order finite difference approximation. The backward finite difference is used to approximate the first-order derivative, while the central difference scheme is used to approximate the second-order derivative. The length of the fixed bed is divided into N_z equally distributed points in z-direction.

As presented in Appendix **??**, all the governing can be written in the integral form using the Divergence Theorem. The integral equation states that the change rate of the integral of any quantity over an arbitrary control volume is given by the flux through the boundary of the control volume, with being the outer surface normal through the boundary. That quantity is neither produced nor consumed inside of the control volume and is hence conserved. For a derivative to be conservative, it must form a telescoping series. In other words, after the addition of all terms coming from the discretization over a grid, only the boundary terms should remain and the artificial interior points should cancel out. To ensure the mass conservation, the discretization is applied on the conservative form of the process model.

2.4. Sensitivity Analysis

Local derivative-based methods involve taking the partial derivative of the output with respect to an input parameter. This set of derivatives, known as sensitivity equations, is solved simultaneously with the process model. The sensitivity analysis aims to investigate how responsive the solution is for the perturbation of the parameter p. As discussed by Dickinson and Gelinas [27], the sensitivity analysis can be used to determine the influence of the uncertainty on the solution of the original system. A sensitivity analysis can be used to distinguish sensitive parameters from insensitive ones, which might be helpful for model reduction. Finally, from a control engineering point of view, the sensitivity analysis allows sorting the control variables with respect to the level of effort required to change the model's output.

As presented in the work of Maly and Petzold [28], the sensitivity analysis equations($\dot{Z}$) are developed by taking the total derivative of the state vector x with respect to parameters p, where p is a subset of the parameter space θ.

$$Z(x(t);p) = \frac{dx(t)}{dp} \tag{28}$$

The new system of equations can be obtained by taking derivatives of Z with respect to time t and applying the chain rule.

$$\dot{Z}(x(t);p) = \frac{dZ(x(t);p)}{dt} = \frac{d}{dt}\left(\frac{dx(t)}{dp}\right) = \frac{d}{dp}\left(\frac{dx(t)}{dt}\right) = \frac{dG(x(t);p)}{dp} \tag{29}$$

The sensitivity equation can be obtained by applying the definition of the total derivative to the Equation 29.

$$\frac{dG(x(t);p)}{dp} = \underbrace{\frac{\partial G(x(t);p)}{\partial x(t)}}_{J_x(x(t);p)} \underbrace{\frac{\partial x(t)}{\partial p}}_{S(x(t);p)} + \underbrace{\frac{\partial G(x(t);p)}{\partial p}}_{J_p(x(t);p)} \tag{30}$$

The sensitivity Equation 30 is solved simultaneously with the original system and is made of three terms: jacobian $J_x(x(t);p)$, sensitivity matrix $S(x(t);p)$ and jacobian $J_p(x(t);p)$. The jacobian $J_x(x(t);p)$ represents the matrix of equations of size $N_x \times N_x$, where each equation $J_x(n_x, n_x)$ is the derivative of process model equations $G_{n_x}(x(t);p)$ with respect to the state variable x_{n_p}.

$$J_x(x(t);p) = \begin{pmatrix} \frac{\partial G_1(x(t);p)}{\partial x_1(t)} & \frac{\partial G_1(x(t);p)}{\partial x_2(t)} & \cdots & \frac{\partial G_1(x(t);p)}{\partial x_{N_x}(t)} \\ \frac{\partial G_2(x(t);p)}{\partial x_1(t)} & \frac{\partial G_2(x(t);p)}{\partial x_2(t)} & \cdots & \frac{\partial G_2(x(t);p)}{\partial x_{N_x}(t)} \\ \vdots & \vdots & \ddots & \vdots \\ \frac{\partial G_{N_x}(x(t);p)}{\partial x_1(t)} & \frac{\partial G_{N_x}(x(t);p)}{\partial x_2(t)} & \cdots & \frac{\partial G_{N_x}(x(t);p)}{\partial x_{N_x}(t)} \end{pmatrix} \tag{31}$$

The sensitivity matrix $S(x(t);p)$ represents the matrix of equations of size $N_x \times N_p$, where each subequation $S(n_x, n_p)$ is the derivative of the state variable x_{n_x} with respect to the parameter p_{n_p}.

$$S(x(t);p) = \begin{pmatrix} \frac{\partial x_1(t)}{\partial p_1} & \frac{\partial x_1(t)}{dp_2} & \cdots & \frac{dx_1(t)}{dp_{N_p}} \\ \frac{\partial x_2(t)}{\partial p_1} & \frac{\partial x_2(t)}{dp_2} & \cdots & \frac{dx_2(t)}{dp_{N_p}} \\ \vdots & \vdots & \ddots & \vdots \\ \frac{\partial x_{N_x}(t)}{\partial p_1} & \frac{\partial x_{N_x}(t)}{dp_2} & \cdots & \frac{\partial x_{N_x}(t)}{dp_{N_p}} \end{pmatrix} \tag{32}$$

The jacobian $J_p(x(t);p)$ represents the matrix of equations of size $N_x \times N_p$, where each subequation $J_p(n_x, n_p)$ is the partial derivative of the process model equation F_{n_x} with respect to the parameter p_{n_p}.

$$J_p(x(t);p) = \begin{pmatrix} \frac{\partial G_1(x(t);p)}{\partial p_1} & \frac{\partial G_1(x(t);p)}{\partial p_2} & \cdots & \frac{\partial G_1(x(t);p)}{\partial p_{N_p}} \\ \frac{\partial G_2(x(t);p)}{\partial p_1} & \frac{\partial G_2(x(t);p)}{\partial p_2} & \cdots & \frac{\partial G_2(x(t);p)}{\partial p_{N_p}} \\ \vdots & \vdots & \ddots & \vdots \\ \frac{\partial G_{N_x}(x(t);p)}{\partial p_1} & \frac{\partial G_{N_x}(x(t);p)}{\partial p_2} & \cdots & \frac{\partial G_{N_x}(x(t);p)}{\partial p_{N_p}} \end{pmatrix} \tag{33}$$

The combined system containing the original set of equations $G(x(t);p)$ and sensitivity equations can be formulated as $\mathbf{G}(x(t);p)$. The size of $\mathbf{G}(x(t);p)$ is equal to $N_s = N_x(N_p + 1)$.

$$\mathbf{G}(x(t);p) = \begin{bmatrix} G(x(t);p) \\ J_x(x(t);p)S(x(t);p) + J_p(x(t);p) \end{bmatrix} \tag{34}$$

The initial conditions are described as

$$\mathbf{G}(x(t_0);p) = \begin{bmatrix} x(t_0), & \frac{dx(t_0)}{dp_1} & \cdots, & \frac{dx(t_0)}{dp_{N_p}} \end{bmatrix}^T \tag{35}$$

The sensitivity analysis of the output function can be performed with respect to parameters p. The output function $g(x(t))$ returns $y(t)$. By taking a total derivative of $y(t)$ with respect to p, the new sensitivity equation can be found.

$$\frac{dy(t)}{dp} = \frac{dg(x(t))}{dp} = \frac{\partial g(x(t))}{\partial x(t)}\frac{\partial x(t)}{\partial p} + \frac{\partial g(x(t))}{\partial p} \tag{36}$$

3. Results

This work investigates the influence of inlet temperature, pressure, and mass flow rate on the state space and the extraction yield. The process model and parameters have been discussed in article 1. The process model was calibrated on the set of experiments obtained at different operating conditions, $30-40°C$, $100-200$ bar, and $3.33-6.67\times10^{-5}$ kg/s. The sensitivity analysis has been performed assuming that the system operates at $35°C$, 150 bar and 5×10^{-5} kg/s.

3.1. Flow rate

The increase in the mass-flow rate affects the system simultaneously along the spatial direction by increasing the velocity but without affecting the thermodynamic state of the fluid. As a result, Figure 5 indicates that the system's pressure remains unaffected by changes in the flow rate.
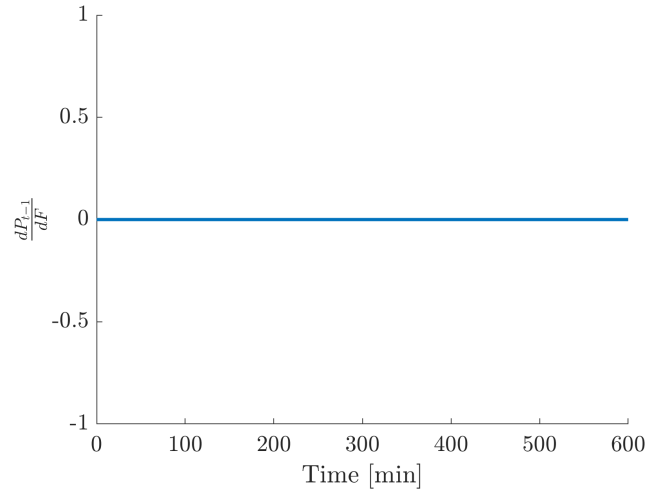
Figure 5: The effect of F change on P

It is important to note that h represents enthalpy but not total enthalpy, thus excluding kinetic energy. As a consequence of the modelling assumptions, changes in h and ρ occur in response to changes in pressure or temperature, which explains no deviation of $h \times \rho$ in Figure 6.

Figure 7 visualizes the local sensitivity of the solute concentration in the solid phase to changes in the mass flow rate during a supercritical fluid extraction process. It is postulated that with an increase in the mass flow rate, the driving force for mass transfer—the concentration gradient—becomes more pronounced, leading to an accelerated decrease in solute concentration within the solid matrix. This is exhibited by the negative sensitivity values: the solute is depleted more rapidly from the solid phase with higher
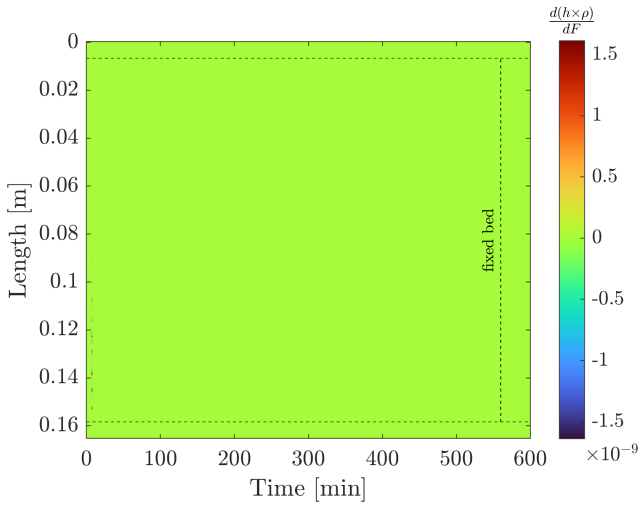
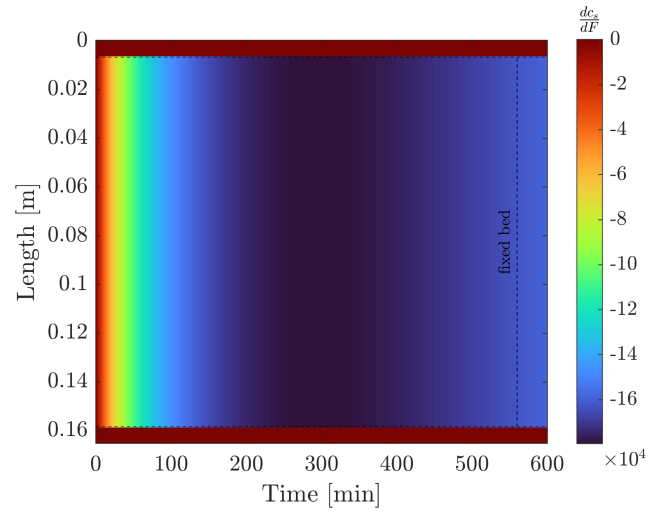**Figure 6:** The effect of F change on $h \times \rho$

Figure 7: The effect of F change on C_s

mass flow rates. The most significant sensitivity is seen at the process commencement, particularly at the column inlet (top left corner with bright colours), where the concentration of solute is highest, and the effect of mass flow rate on extraction is most pronounced.

As the extraction progresses, the sensitivity values become less negative, moving towards zero, depicted by the gradient transitioning to cooler colors towards the bottom of the figure. This gradual change corresponds to the decreasing concentration of the solute in the solid phase, which results in a diminishing concentration gradient and, consequently, a reduction in the rate of extraction. The sensitivity approaching zero suggests that the driving force for mass transfer is decreasing as the solute is being depleted.

The asymptotic approach to zero sensitivity indicates a physical plateau in the extraction process, where further increases in mass flow rate no longer enhance the extraction efficiency. In practical terms, this asymptotic behavior signifies the approach towards an extraction endpoint where the remaining solute concentration in the solid phase is minimal and becomes less dependent on the mass flow rate. At this stage, other factors, such as diffusion within the solid matrix or equilibrium limitations, may limit the extraction rate.

In the most extreme cases, depicted by the uniform regions in the plot, the solute has been effectively exhausted, and the remaining traces in the solid phase are no longer influenced by changes in the mass flow rate. This stage represents the final equilibrium, where the concentration gradient effectively drops to zero, rendering the mass flow rate inconsequential for the extraction of the remaining solute. At this juncture, the system has reached its thermodynamic limit, and the efficiency of extraction cannot be enhanced by merely increasing the flow rate. This underscores the importance of optimizing the mass flow rate at the beginning and throughout the extraction process to ensure efficient solute recovery before reaching this terminal stage.

The Figure 8 depicts the sensitivity of the solute concentration in the fluid phase to the flow rate within a supercritical fluid extraction system. This sensitivity analysis reveals how the solute's behavior in the fluid phase is influenced by variations in the flow rate over the course of the extraction process, as depicted by both time and the length of the extraction column.

In the initial phase of the extraction, the sensitivities near the inlet are negligible, as shown by the colors being close to zero. This indicates a minimal initial response to changes in the flow rate, which could be due to the presence of an high concentration gradient, allowing the fluid phase to rapidly reach solute regardless of the flow rate.

As the extraction progresses, positive sensitivities emerge along the length of the extractor, indicated by the concentration front that develops and moves along the flow direction. This front represents the increased movement of the solute with the fluid phase as the flow rate increases, suggesting an enhanced mass transfer due to the elevated velocity of the supercritical fluid. This velocity increase augments the concentration gradient, thus encouraging a more efficient solute migration from the solid to the fluid phase.

Following the positive front, there is an emergence of a front characterized by negative sensitivities. This trend illustrates a diminishing solute concentration in the fluid phase, and it reflects a point in the extraction where the solute availability in the solid phase becomes a limiting factor; the depletion of solute reduces the concentration gradient, thereby decelerating the extraction rate.

Toward the end of the extraction process, the sensitivities are shown to increase from their negative values towards zero. This asymptotic approach suggests that the system is reaching a kinetic regime where further increases in the flow rate have a low impact on the solute concentration in the fluid phase. This behavior reflects a physical limit where the remaining solute in the solid phase is insufficient to sustain a high concentration in the fluid phase, regardless of the flow

rate. It indicates a terminal phase of the extraction process where the available solute has been largely exhausted, and the system response to changes in flow rate is inherently constrained by the depletion of extractable material.
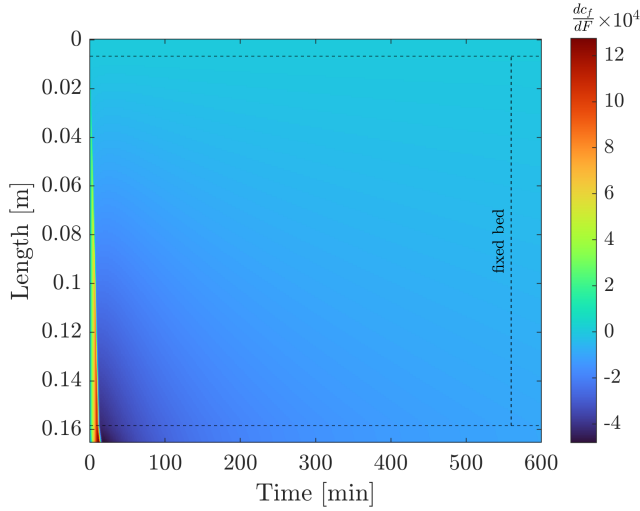

Figure 8: The effect of F change on C_f

The Figure 9 depicts the sensitivity of the extraction yield to variations in mass flow rate as a function of time. The curve's initial rise to a peak followed by a decline conveys the dynamic relationship between the mass flow rate and the extraction yield within the supercritical extraction process.

In the early phase, the sensitivity is minimal, denoting that adjustments to the mass flow rate have a negligible influence on the yield. This can be attributed to the initial phase of the extraction, where the mass transport mechanisms are mainly controlled by a high concentration gradient.

As the process evolves, the curve's ascent to its apex signifies a period during which the extraction yield becomes increasingly sensitive to the mass flow rate. This is likely due to the mass flow rate enhancing the convective transport of solute, maximizing the extraction efficiency. At this stage, the solute transfer from the solid to the fluid phase is most responsive to changes in flow rate.

However, the curve's descent past the peak suggests a diminishing return on sensitivity with further increases in mass flow rate. The decrease indicates a transitional phase where the extraction process likely encounters diffusion limitations or a depletion of readily extractable solute. The concentration gradient, which drives the mass transfer, may be reduced due to the depletion of solute in the solid phase, or the system may be experiencing diffusive resistances that limit the rate at which solute can be delivered to the fluid phase.

The asymptotic approach to zero sensitivity towards the end of the curve reflects a regime where the yield is no longer significantly influenced by the mass flow rate. At this juncture, the extraction process has likely exhausted the available solute, and any further increase in mass flow rate does not result in a proportional increase in yield.

The extraction system has reached a point of saturation or equilibrium where the mass transfer is limited by factors other than flow rate, such as the intrinsic properties of the solute or the matrix, indicating that the system has achieved as much extraction as is practically feasible under the given conditions.

The curve captures the non-linear and transient nature of the extraction yield's response to the mass flow rate, underscoring the importance of optimizing flow rates over the duration of the extraction to maximize yield. It also highlights the multifaceted dependencies and constraints inherent in supercritical fluid extraction processes, such as mass transfer rates, solute availability, and diffusion limitations.
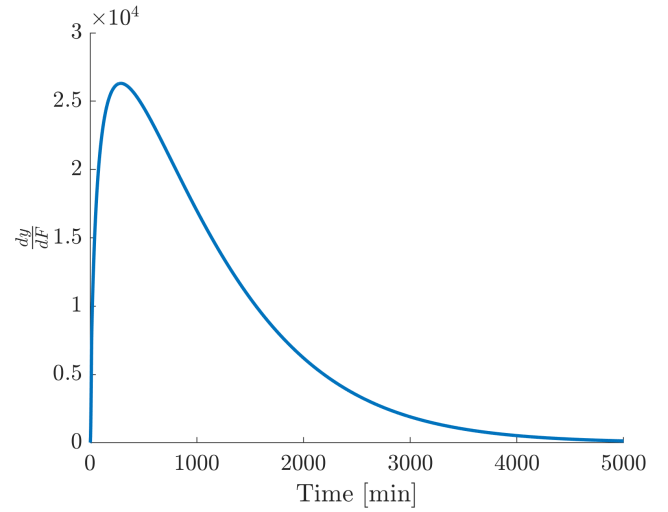

Figure 9: The effect of F change on $y(t)$

3.2. Pressure

As discussed in Chapter 2.2, a small pressure wave propagates at the speed of sound relative to the flow. If the flow velocity is relatively low, all pressure changes are hydrodynamic (resulting from velocity motion) rather than thermodynamic. The Low Mach-number assumption leads to instant propagation of the thermodynamic pressure throughout the system. This assumption allows considering a single pressure value for the entire system, as all changes occur simultaneously within the machine. Figure 10 illustrates a step function representing the pressure change.

According to Equation 21, the pressure change directly affects the quantity $h \times \rho$ through $\partial(P(t)A_f)/\partial t$, leading to the step change along the whole system, as presented in Figure 11. The uniform response across the entire extraction column length and time, represented by the homogeneously dark red color, indicates that the entire system experiences an immediate and uniform change in enthalpy density in response to pressure changes. This is consistent with the physical expectation that pressure changes should equilibrate rapidly throughout the fluid phase due to the high compressibility of supercritical fluids.
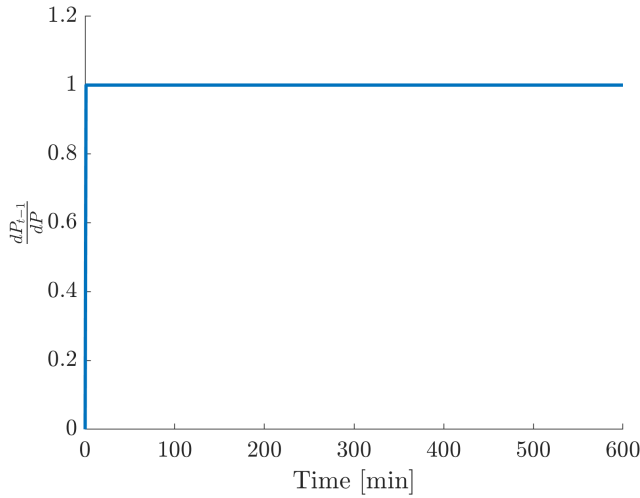
Figure 10: The effect of P change on P in the system

As discussed in Chapter 2.3.1, the velocity of a fluid is inversely related to its density, which suggests that with higher fluid density—often associated with increased pressure—the velocity decreases. This leads to an extended residence time of the fluid within the system. The lower velocity afforded by increased pressure allows for a longer interaction between the solute and the solvent, potentially a higher concentration of solute in the fluid phase.

Simultaneously, pressure changes alter the fluid's thermodynamic state, affecting the extraction process's kinetics. These changes are characterized by correlations (article 1), such as the increase of the diffusion coefficient D_i^R with fluid density. A higher D_i^R indicates enhanced mass transfer capabilities, contributing to an increased rate of extraction.

Figure 12 captures these dual effects on the solute concentration within the solid matrix. Initially, the system response is low due to a high concentration gradient. When the concentration gradient starts to diminish, high sensitivities reveal that changes in pressure have a more pronounced effect. This is consistent with the fluid's higher density and lower velocity, resulting in more effective mass transfer from the solid to the fluid phase.

Over time, the pressure change has a lower effect and the sensitivities decay. This trend signifies that the impact of pressure on solute concentration is diminishing, likely due to the depletion of the solute in the solid phase over time. The decreasing concentration gradient suggests that the solute availability becomes a limiting factor in the extraction process.

Eventually, sensitivities asymptotically approach zero. The solute concentration in the solid phase has been reduced, and further changes in pressure do not influence the remaining concentration. This behaviour reflects that in the later extraction phase, the kinetics of extraction are dominated by the reduced availability of the solute rather than the conditions of the supercritical fluid.

Regarding the boundary conditions, by applying the Dirichlet boundary conditions(mean setting a fixed temperature at the system boundary) can leads to a possible thermal gradient within the system if the initial temperatures differ. In contrast, Neumann boundary conditions would dictate that the heat flux at the boundaries be held constant, ensuring temperature uniformity between the inlet and the rest of the extractor. In case of this work, the Neumann boundary conditions have been applied, as indicated by the uniform response in enthalpy density, implying that there is no temperature gradient caused by a heat front propagating through the system. Instead, the temperature within the extractor is instantaneously and evenly matched to that at the inlet.
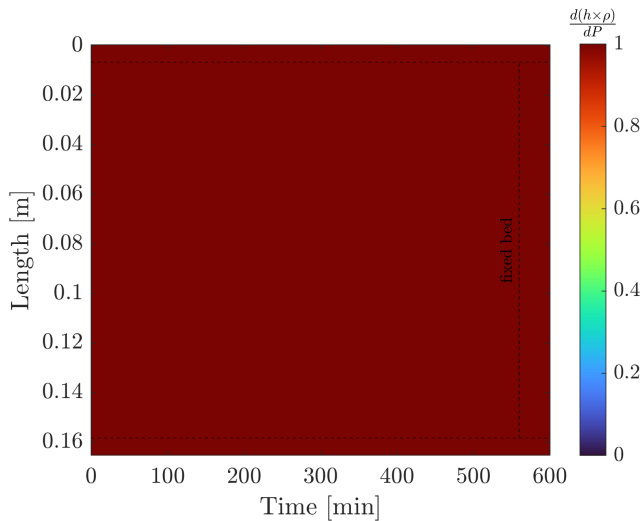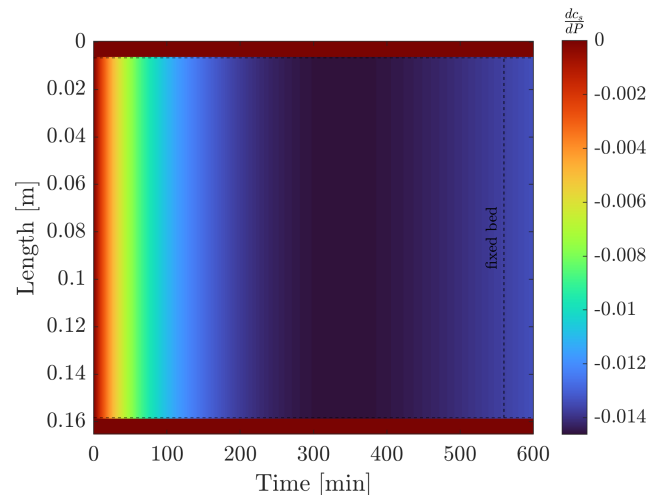

Figure 11: The effect of P change on $(h \times \rho)$ in the system

The provided figure showcases the sensitivity of the solute concentration in the solid phase with respect to changes in pressure throughout a fixed bed in a supercritical fluid extraction process.

Figure 12: The effect of P change on C_s

Figure 13 shows the sensitivity of the solute concentration in the fluid phase as a function of pressure changes

throughout the supercritical extraction column's length and over the extraction process's duration. An increase in pressure typically enhances the solute's solubility, resulting in its heightened presence in the supercritical fluid, which is seen as a leading front moving through the system. Due to the diffusion effect, the gradient becomes more dispersed in regions beyond the fixed bed. Following this, the formation of a trailing front characterized by decreasing sensitivities can be observed. This trailing front can be explained by the decrease in the concentration gradient as the solute is increasingly extracted and the available concentration within the solid phase diminishes. As seen in the figure, sensitivities are declining towards zero. This asymptotic trend suggests the driving force for the mass transfer—the concentration gradient—has been minimized, and changes in pressure no longer significantly impact the solute concentration in the fluid phase.
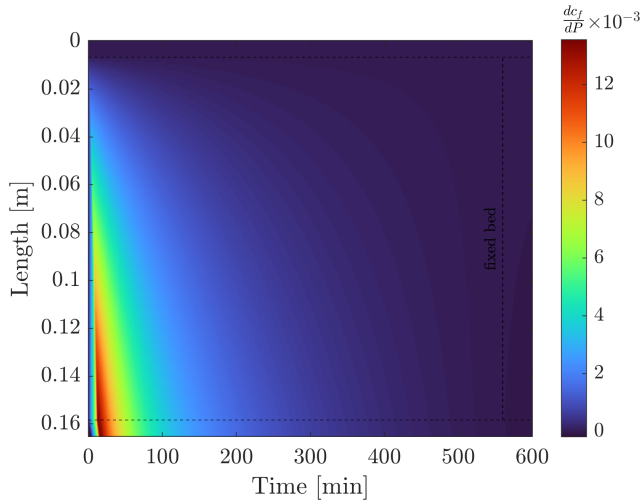
phase: as the available solute in the solid phase diminishes, the potential for further increasing the yield through pressure alone is reduced. The remaining solute concentration becomes a limiting factor, and the mass transfer driving force, initially augmented by pressure, no longer plays a dominant role.
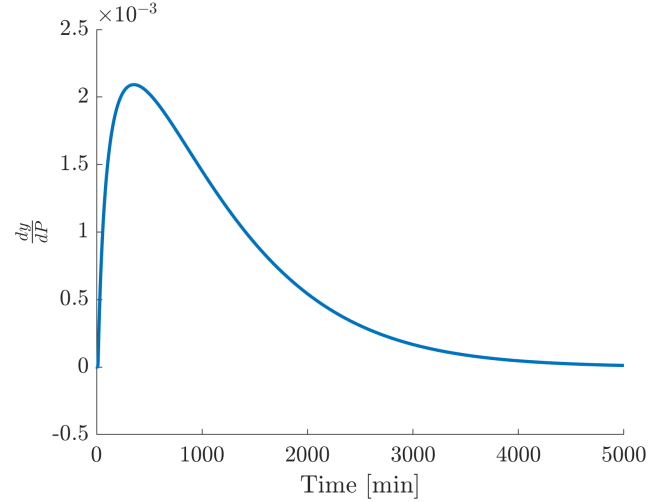

Figure 14: The effect of P change on $y(t)$

Figure 13: The effect of P change on C_f

Figure 14 illustrates the temporal evolution of the extraction yield's sensitivity to changes in pressure within a supercritical fluid extraction system.

Initially, the curve displays an almost flat profile, suggesting a latency in the system's response to pressure changes. A minor initial decrease in sensitivity, indicated by a slight dip below zero, may arise due to a decrease in the velocity of the fluid phase. For a constant mass flow rate, an increase in fluid density due to heightened pressure results in a lower fluid velocity, potentially leading to this reduced sensitivity.

As the process continues, the curve ascends sharply, indicating a positive yield response to pressure. This increase in sensitivity can be associated with the enhanced solubility and mass transfer capabilities imparted by higher pressures, improving the rate at which solute is extracted into the fluid phase. The peak in dy/dP reflects the most responsive period of the system, where pressure changes are highly effective in improving yield.

Beyond the peak, the sensitivity declines, converging towards zero. This descending curve represents a depletion

3.3. Inlet temperature

The sensitivity analysis of the inlet temperature differs from the two cases presented earlier because the perturbation does not affect the entire system instantaneously; instead, it propagates through it.

Figure 15 presents the sensitivity of the system's pressure response to changes in the inlet temperature over time during a supercritical fluid extraction process. The flat curve, hovering at zero, indicates a system where the pressure does not exhibit any response to changes in the inlet temperature throughout the entire operation period. In other words, the extraction system maintains a constant pressure regardless of any fluctuations in the temperature of the fluid entering the system. The invariance in pressure displayed in the Figure 15 corroborates the model assumptions discussed in the Chapter X, where the pressure is assumed to be a control variable.

Figure 16 displays the sensitivity of the fluid enthalpy density to changes in the inlet temperature across the extraction bed over time. Given that the Dirichlet boundary conditions are applied to the system, any alteration in inlet temperature will have an immediate and localized effect on the enthalpy density at the entrance of the extraction column on the fluids enthalpy. This alteration results in a heat front propagation from the inlet to the outlet of the extractor as presented on the Figure 16. As time progresses, the impact of the inlet temperature on enthalpy diminish and the sensitivities converging towards zero. This convergence suggests that the system is reaching a new thermal equilibrium. The uniformity of the enthalpy at later times implies that the initial temperature perturbations have equilibrated
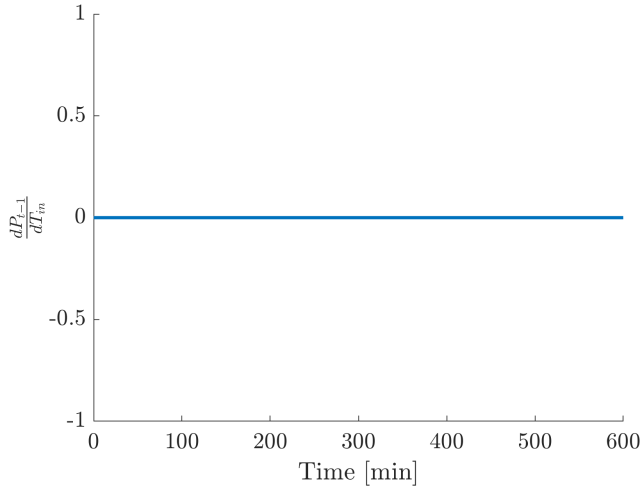
Figure 15: The effect of T_{in} change on P in the system

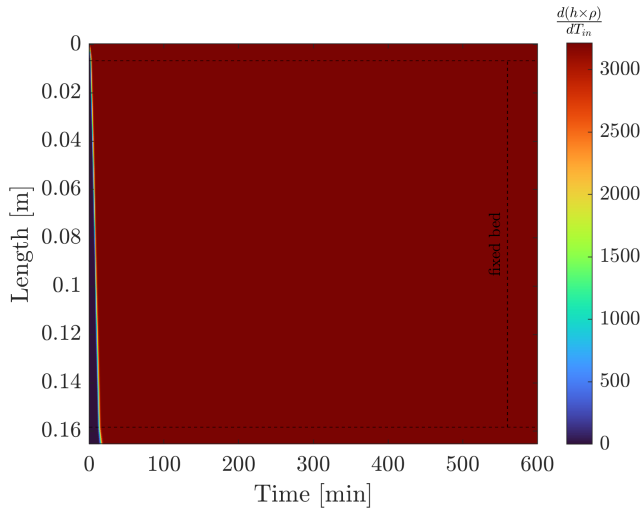throughout the bed, and the system has adapted to the new inlet temperature condition.

Figure 16: The effect of T_{in} change on $(h \times \rho)$ in the system

Figure 17 shows the temporal and spatial sensitivity of the solute concentration in the solid phase to changes in the inlet temperature during a supercritical fluid extraction process. The positive sensitivities observed suggest that the solute concentration in the solid phase increases with rising inlet temperature. This initial increase could be attributed to a reduction in solute solubility in the supercritical fluid at higher temperatures or a slowdown in mass transfer kinetics. As presented in article 1, a rise in temperature at constant pressure would increase solute diffusivity D_i^R in supercritical fluids; however, the increase in concentration in the solid phase indicates other dominating factors, such as changes in solubility described by the solubility parameter (Υ), which might decrease, thereby reducing the extraction rate.

As the extraction progresses, the sensitivities flatten out and then decrease. Towards the end of the extraction period,

the sensitivities approach a positive constant, implying that the effect of inlet temperature on the concentration of the solute in the solid phase becomes negligible. This behaviour can be explained if it assumed that the extraction kinetic slowed because at the high temperature, which leads to higher concentration gradient in the later part of the process. The reduced availability of extractable solute in the later part of the process corresponds to the diminishing of the sensitivity.
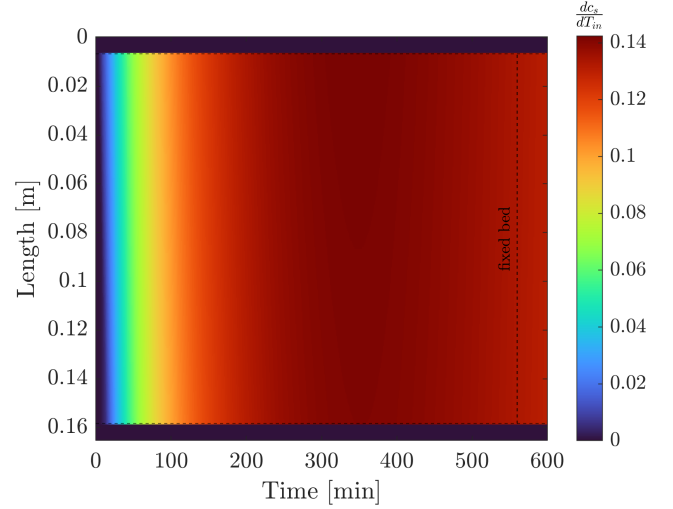

Figure 17: The effect of T_{in} change on C_s in the system

The Figure 18 represents the sensitivity of the concentration of solutes in the fluid phase over a period of 600 minutes as a result of changes in the inlet temperature. In the initial phase of the process, indicated by the area where sensitivities are at or near zero, there is a lack of response, likely reflecting an idle period or delay as the system adjusts to the new inlet temperature. This could represent the time needed for the thermal front to propagate through the system and influence the solubility and mass transfer rates of the solutes. As the warmer fluid begins to interact with the solid phase, the negative sensitivities are observed. These negative values imply a decrease in solute concentration within the fluid phase, which might be attributed to a reduced diffusion coefficient (D_i^R) due to increased fluid viscosity at higher temperatures, or possibly due to a change in the solubility (Υ) of the solute with temperature. If the solubility decreases with temperature for the given solute, an increase in temperature could indeed result in a lower solute concentration in the fluid phase. Later the sensitivities starts to increase due higher concentration gradient if compared to before the temperature change. Towards the end of the time period, the figure shows the sensitivities stabilizing at a constant value. Eventually, the system response stabilize around a constant value when the extraction kinetics become a limiting factor.

Figure 19 shows the time-dependent response of the extraction yield's sensitivity to changes in the inlet temperature. Initially, there is no change in yield as the heat front
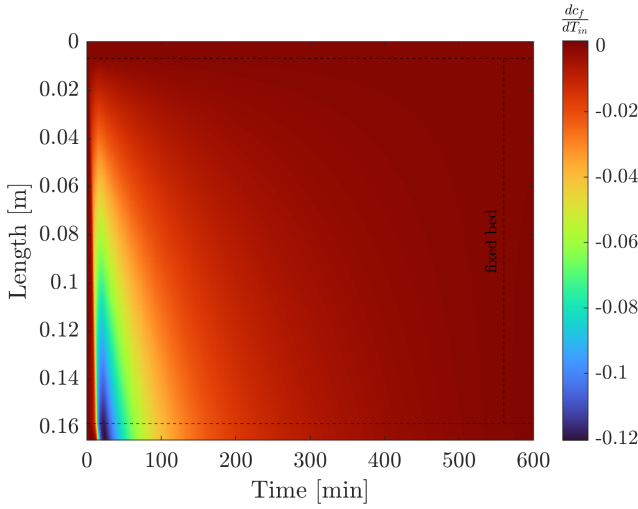
Sensitivity Analysis

Figure 18: The effect of T_{in} change on C_f in the system

Figure 19: The effect of T_{in} change on $y(t)$ in the system

needs to propagate the along the system. That delayed response, cause the yield sensitivity to stay flat at the beginning of the extraction.

As the system starts responding, a small increase in sensitivity can be observed, which indicates a transient enhancement in yield. This is due to the velocity of the fluid, which is inversely proportional to density. The sensitivity peak comes from the fact that the fluid moves faster across the system, while the mass transfer kinetic is mainly driven by high concentration gradient.

Subsequently, the sensitivity curve descends into negative territory, suggesting that the increased inlet temperature eventually reduces the extraction efficiency. As explained above, due to complex relation between temperature and various mass transfer parameters, including the solubility of different compounds and the diffusivity within the supercritical fluid, the temperature increase might have a negatively affected on the extraction efficiency. The minimum point reached by the sensitivity curve implies a period where the yield is affected the most by the temperature increase.

Afterward, the curve's gradual ascent towards zero reflects a stabilizing effect. The curve eventually flattens out, maintaining a slightly negative sensitivity, suggesting that while the system has reached a new quasi-steady state. The overall yield remains slightly compromised compared to the baseline. At this point, the extraction process is limited by availability of the solute in the solid particles. This extended simulation offers a comprehensive view of how inlet temperature variations can impact the extraction yield over time.

4. Conclusions

The sensitivity analysis is a tool to understand the parametric dependence in the dynamic behaviour of the analysed system. The presented formulation involves derivative-based local sensitivity analysis of the model solution with respect to selected parameters and controls. The sensitivity
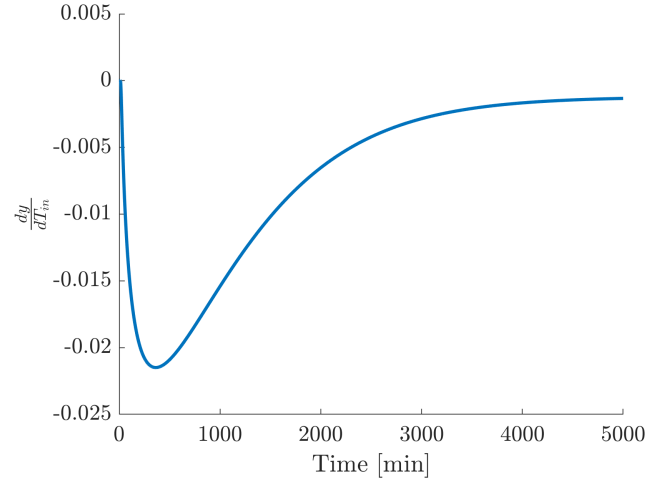
equations can be obtained in various ways, but the automatic differentiation technique was implemented to obtain the sensitivity equations in this work. By identifying which parameters are influential at each period of the simulation, local sensitivity analysis can yield valuable information for guiding the process modelling, the design of experiments or the model reduction. The local sensitivity analysis techniques consider the sensitivities at only a small region of parameter space, and the conclusions derived from such an analysis are limited to local conditions unless the discussed system is a linear model.

In this study, the local sensitivity analysis method was introduced to explore the dynamics of the supercritical extraction system, which consists of a set of partial differential equations. The sensitivity equations evaluate the influence of control variables such as flow rate, pressure, and inlet temperature on the state-space consisting of the concentration of the solute in solid and liquid phases, the fluid's enthalpy density, system pressure, and extraction yield. Every change in the control variables leads to a state-space change, eventually affecting the process performance.

Similarities between Figures 9, 14 and 19 can observed, although the sources of disturbances are different. All the plots stay initially plat, and this is because the extraction kinetic is mainly controlled by the concentration gradient. The largest sensitivity deviations are observed in the second extraction phase, which is mainly controlled by the internal mass transfer. These deviations are strongly related to the fluid velocity and the correlations used to connect the extraction kinetic parameters. As correlations used in this work are linear functions of the fluid density(article 1), Figures 14 and 19 are characterised by the opposite changes in the fluid density, which leads to the sensitivity plots with similar shape but opposite sign. In the third extraction phase, the concentration gradient and the internal diffusion coefficient decrease with the solute concentration in the solid phase(it is more difficult to extract the solute from the particle core than from the outer shell). It is important to note that the

local-sensitivity methods obtain the discussed results, which can be obtained at different operating conditions.

This information can be utilized to identify which control variables influence the extraction yield the most. The controls with high sensitivities on the extraction can be used to investigate to find optimal operating conditions from an economic point of view.

References

[1] Ompal Singh, Zakia Khanam, Neelam Misra, and Manoj Kumar Srivastava. Chamomile (matricaria chamomilla l.): An overview. Pharmacognosy Reviews, 5(9):82, 2011. ISSN 0973-7847. doi: 10.4103/0973-7847.79103.

[2] Janmejai Srivastava. Extraction, characterization, stability and biological activity of flavonoids isolated from chamomile flowers. Molecular and Cellular Pharmacology, 1(3):138–147, August 2009. ISSN 1938-1247. doi: 10.4255/mcpharmacol.09.18.

[3] Anne Orav, Ain Raal, and Elmar Arak. Content and composition of the essential oil ofchamomilla recutita(l.) rauschert from some european countries. Natural Product Research, 24(1):48–55, January 2010. ISSN 1478-6427. doi: 10.1080/14786410802560690.

[4] Ernesto Reverchon, Giorgio Donsi, and Libero Sesti Osseo. Modeling of supercritical fluid extraction from herbaceous matrices. Industrial & Engineering Chemistry Research, 32(11):2721–2726, nov 1993. doi: 10.1021/ie00023a039.

[5] H. Sovova. Rate of the vegetable oil extraction with supercritical co2. modelling of extraction curves. Chemical Engineering Science, 49 (3):409–414, 1994. doi: 10.1016/0009-2509(94)87012-8.

[6] E. Reverchon. Mathematical modeling of supercritical extraction of sage oil. AIChE Journal, 42(6):1765–1771, June 1996. ISSN 1547-5905. doi: 10.1002/aic.690420627.

[7] L. Fiori, D. Calcagno, and P. Costa. Sensitivity analysis and operative conditions of a supercritical fluid extractor. The Journal of Supercritical Fluids, 41(1):31–42, may 2007. doi: 10.1016/j.supflu.2006.09.005.

[8] M.M. Santos, E.A. Boss, and R. Maciel Filho. Supercritical extraction of oleaginous: parametric sensitivity analysis. Brazilian Journal of Chemical Engineering, 17(4–7):713–720, December 2000. ISSN 0104-6632. doi: 10.1590/s0104-66322000000400035.

[9] Tahmasb Hatami and Ozan N. Ciftci. Techno-economic sensitivity assessment for supercritical co2 extraction of lycopene from tomato processing waste. The Journal of Supercritical Fluids, 204:106109, January 2024. ISSN 0896-8446. doi: 10.1016/j.supflu.2023.106109.

[10] Massimo Poletto and Ernesto Reverchon. Comparison of models for supercritical fluid extraction of seed and essential oils in relation to the mass-transfer rate. Industrial & Engineering Chemistry Research, 35(10):3680–3686, January 1996. ISSN 1520-5045. doi: 10.1021/ie9600093.

[11] J Elliott. Introductory chemical engineering thermodynamics. Prentice Hall, Upper Saddle River, NJ, 2011. ISBN 9780136068549.

[12] G. G. Simeoni, T. Bryk, F. A. Gorelli, M. Krisch, G. Ruocco, M. Santoro, and T. Scopigno. The widom line as the crossover between liquid-like and gas-like behaviour in supercritical fluids. Nature Physics, 6(7):503–507, jun 2010. doi: 10.1038/nphys1683.

[13] Daniel Banuti. The latent heat of supercritical fluids. Periodica Polytechnica Chemical Engineering, 63(2):270–275, jan 2019. doi: 10.3311/ppch.12871.

[14] W. Sheng, G. J. Chen, and H. C. Lu. Prediction of transport properties of dense gases and liquids by the peng-robinson (PR) equation of state. International Journal of Thermophysics, 10(1):133–144, jan 1989. doi: 10.1007/bf00500714.

[15] Sydney Chapman and T. G. Cowling. The Mathematical Theory of Non-uniform Gases. Cambridge University Press, 1991. ISBN 9780521408448.

[16] A. Fenghour, William A. Wakeham, and V. Vesovic. The viscosity of carbon dioxide. Journal of Physical and Chemical Reference Data, 27 (1):31–44, jan 1998. doi: 10.1063/1.556013.

[17] Arno Laesecke and Chris D. Muzny. Reference correlation for the viscosity of carbon dioxide. Journal of Physical and Chemical Reference Data, 46(1):013107, mar 2017. doi: 10.1063/1.4977429.

[18] M. L. Huber, E. A. Sykioti, M. J. Assael, and R. A. Perkins. Reference correlation of the thermal conductivity of carbon dioxide from the triple point to 1100 k and up to 200 MPa. Journal of Physical and Chemical Reference Data, 45(1):013102, mar 2016. doi: 10.1063/1.4940892.

[19] John D. Anderson. Computational fluid dynamics the basic with applications. McGraw-Hill, 1995. ISBN 9780071132107.

[20] Stefan Schreier. Compressible flow. Wiley, 1982. ISBN 047105691X.

[21] N. R. Bulley, M. Fattori, A. Meisen, and L. Moyls. Supercritical fluid extraction of vegetable oil seeds. Journal of the American Oil Chemists' Society, 61(8):1362–1365, aug 1984. doi: 10.1007/bf02542243.

[22] M. Spiro and M. Kandiah. Extraction of ginger rhizome: partition constants and other equilibrium properties in organic solvents and in supercritical carbon dioxide. International Journal of Food Science & Technology, 25(5):566–575, jun 2007. doi: 10.1111/j.1365-2621.1990.tb01116.x.

[23] Helena Sovova. Broken-and-intact cell model for supercritical fluid extraction: Its origin and limits. The Journal of Supercritical Fluids, 129:3–8, nov 2017. doi: 10.1016/j.supflu.2017.02.014.

[24] Motonobu Goto, Bhupesh C. Roy, and Tsutomu Hirose. Shrinking-core leaching model for supercritical-fluid extraction. The Journal of Supercritical Fluids, 9(2):128–133, jun 1996. doi: 10.1016/s0896-8446(96)90009-1.

[25] Jürgen Gmehling, Michael Kleiber, Bärbel Kolbe, and Jürgen Rarey. Chemical Thermodynamics for Process Simulation. Wiley, mar 2019. doi: 10.1002/9783527809479.

[26] H. Sovova, R. Komers, J. Kucuera, and J. Jezu. Supercritical carbon dioxide extraction of caraway essential oil. Chemical Engineering Science, 49(15):2499–2505, aug 1994. doi: 10.1016/0009-2509(94)e0058-x.

[27] Robert P. Dickinson and Robert J. Gelinas. Sensitivity analysis of ordinary differential equation systems—a direct method. Journal of Computational Physics, 21(2):123–143, jun 1976. doi: 10.1016/0021-9991(76)90007-3.

[28] Timothy Maly and Linda R. Petzold. Numerical methods and software for sensitivity analysis of differential-algebraic systems. Applied Numerical Mathematics, 20(1-2):57–79, feb 1996. doi: 10.1016/0168-9274(95)00117-4.